Review of Scientific Instruments

RESEARCH ARTICLE | AUGUST 04 2023

Time-resolved electron paramagnetic resonance spectrometer based on ultrawide single-sideband phase-sensitive detection

Shixue Zhang; Shengqi Zhou; Jianqing Qi ; Lei Jiao ; Xingwei Guo

Rev Sci Instrum 94, 084101 (2023)
https://doi.org/10.1063/5.0143480

AIP Publishing

Review of Scientific Instruments ARTICLE pubs.aip.org/aip/rsi

Time-resolved electron paramagnetic resonance spectrometer based on ultrawide single-sideband phase-sensitive detection

Cite as: Rev. Sci. Instrum. 94, 084101 (2023); doi: 10.1063/5.0143480
Submitted: 24 January 2023 • Accepted: 18 July 2023 •
Published Online: 4 August 2023

Shixue Zhang, Shengqi Zhou, Jianqing Qi, Lei Jiao, and Xingwei Guo[a)]

AFFILIATIONS

Center of Basic Molecular Science, Department of Chemistry, Tsinghua University, Beijing 100084, China

[a)]Author to whom correspondence should be addressed: xingwei_guo@mail.tsinghua.edu.cn

ABSTRACT

A time-resolved electron paramagnetic resonance (TREPR) method with 40 ns time resolution and a high sensitivity suitable for the detection of short-lived radicals under thermal equilibrium is developed. The key is the introduction of a new detection technique named ultrawide single sideband phase sensitive detection (U-PSD) to the conventional continuous-wave EPR, which remarkably enhanced the sensitivity for the detection of broadband transient signals compared with the direct detection protocol. By repeatedly triggering a transient kinetic event $f(t)$ (e.g., by laser flash photolysis) under a 100 kHz magnetic field modulation with precise phase control, this technique can build an ultrawide single sideband modulated signal. After single sideband demodulation, the flicker noise-suppressed signal $f(t)$ with wide bandwidth is recovered. A U-PSD TREPR spectrometer prototype has been built, which integrated timing sequence control, laser flash excitation, data acquisition systems, and the U-PSD algorithm with a conventional continuous-wave EPR. It exhibited excellent performance in monitoring a model transient radical system, laser flash photolysis of benzophenone in isopropanol. Both the intense chemically induced dynamic electron polarization signals and the much weaker thermal equilibrium EPR signals of the generated acetone ketyl radical and benzophenone ketyl radical were clearly observed within a wide timescale ranging from sub-microsecond to milliseconds. This prototype validated the feasibility of the U-PSD technique and demonstrated its superior performance in studying complex photochemical systems containing various transient radicals, which complements the established TREPR techniques and provides a powerful tool for deep mechanistic understandings, such as in photoredox catalysis and artificial photosynthesis.

I. INTRODUCTION

Time-resolved electron paramagnetic resonance (TREPR) is a powerful technique that enables direct observation and tracking of short-lived (transient) open shell species, such as free radicals and triplet excited states.[1–3] TREPR has been widely applied in the studies of spin dynamics,[4,5] radical chemistry,[6,7] material science,[8,9] and biochemistry.[10,11] Time resolution and sensitivity are crucial factors that determine the power of this technique. Currently, there are two major types of TREPR methods, i.e., direct detection (DD) continuous-wave (CW) TREPR[6,12] and pulsed-microwave Fourier transform (FT) EPR,[11] able to reach cavity bandwidth-limited time resolution (50 and 10 ns, respectively). In principle, both DD CW-TREPR and FT-EPR methods are based on the direct detection technique, which brings about inherently low sensitivity, especially in the time domain where flicker noise is dominant (above a few microseconds). As a result, DD CW-TREPR and FT-EPR are mainly used to detect intense signals, such as free radicals with chemically induced dynamic electron spin polarization (CIDEP),[13,14] and they have gained limited utility in tracing short-lived radicals under thermal equilibrium (i.e., Boltzmann population of the spin state).

Phase sensitive detection (PSD) has been proven a powerful technique that can dramatically improve the sensitivity of steady-state (SS) CW-EPR.[15] However, the inadequate response time (200 μs for a typical commercially available spectrometer) limited the application of the PSD technique in TREPR to enhance the sensitivity. In the past decades, some techniques had been developed to tackle this problem, including high-frequency phase sensitive detection (HF-PSD) EPR[16–18] and broadband phase-sensitive detection (B-PSD) EPR.[19] HF-PSD EPR enhanced the time resolution to 1–2 μs by increasing the field modulation frequency to an upper

limit of 1–2 MHz, albeit with compromised sensitivity due to limited modulation amplitude. The B-PSD EPR technique broke the limitation of time resolution by PSD response time and field modulation frequency, which applied a high-pass filter together with a random phase averaging method under 200 kHz field modulation instead of a traditional lock-in amplifier. However, distortions were observed in the first few microseconds of signal due to missing frequency components caused by the high-pass filter, severely limiting the practical time resolution of this method. To date, a TREPR detection method with both cavity-limited time resolution (10–50 ns) and high sensitivity has been challenging but greatly sought after. The desired TREPR technique would enable radical chemists to address mechanistic challenges that cannot be tackled with the more commonly used transient UV-Vis absorption spectroscopy.

Herein, we report a new technique, referred to as ultrawide single sideband phase-sensitive detection (U-PSD), as well as its application in TREPR. It is important to note that the term "ultrawide" emphasizes a crucial characteristic of this technique, which is the absence of practical signal bandwidth limitations imposed by the modulation frequency. This sets it apart from the B-PSD technique proposed by de Jager. The spectrometer based on this technique is able to trace transient EPR signals with both high time resolution (down to 40 ns) and satisfactory sensitivity (enabling the detection of transient radicals with spins following the Boltzmann distribution) over a wide timescale (from hundreds of nanoseconds to milliseconds). This feature makes it suitable for the study of transient radical species with a wide range of lifetimes, which is a typical scenario in radical chemistry. The instrumentation has minimum hardware requirements compared with a conventional CW-EPR, which complements the existing TREPR techniques and provides a powerful tool for radical chemistry research.

II. THE PRINCIPLE OF ULTRAWIDE SINGLE SIDEBAND PHASE-SENSITIVE DETECTION

A. Basic principle

The desired time-resolved detection method with both high time resolution and high sensitivity over a wide time window should exhibit wide bandwidth and, most importantly, excellent flicker noise (1/*f* noise) suppression ability. However, clean separation of broadband weak signals from the 1/*f* noise is rather challenging, and such techniques remain elusive [Fig. 1(a)].

Application of the traditional PSD technique to pick out signals with an ultrawide bandwidth (from DC to a frequency much higher than the modulation frequency applied) from the 1/f noise does not actually work.[6] Based on the principles of PSD, field modulation (at the frequency of ω_{mod}) shifts the signal of interest out of the 1/f noise region to a less noisy higher frequency domain. For signals with a narrow bandwidth (e.g., steady state signal), clean separation of the target signal from 1/f noise can be achieved. However, for broadband signals, the situation is different. For instance, a fast-evolving signal *f(t)* can be expressed by its Fourier form,

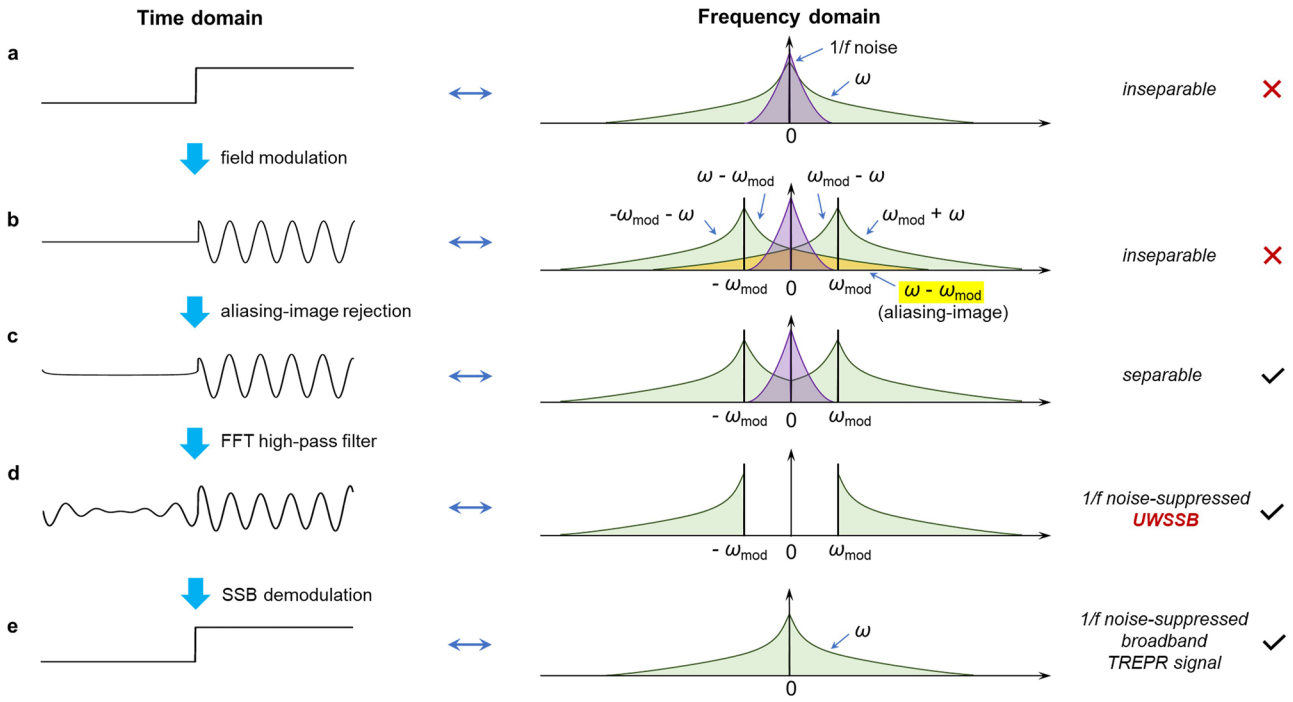

FIG. 1. The principle of the ultrawide single sideband phase sensitive detection (U-PSD). (a) Step signal, (b) aliasing image mixing with both sidebands resulted by field modulation, (c) signal after an aliasing image-rejection procedure, (d) ultrawide single sideband signal after FFT high-pass filter, and (e) the recovered signal by U-PSD.

$$f(t) = \frac{1}{2\pi}\int_{-\infty}^{+\infty} a(\omega)e^{i[\omega t+\varphi(\omega)]}d\omega, \quad (1)$$

which includes various frequency components (ω) with an ultrawide distribution. Field modulation-based EPR detection results in amplitude modulation of the signal, and an ultrawide double sideband signal distributed around ω_{mod} is obtained with severe overlapping in the frequency domain [Fig. 1(b)]: not only does the lower sideband signal overlap with the $1/f$ noise in low frequency region but also its aliasing image mixes with both sidebands. In this case, a clean upper sideband could neither be isolated by simply applying a high-pass filter as is commonly used in telecommunications, nor by a Hartley single sideband modulator as the baseband signal (target transient signal to be detected in this scenario) alone is not available.

We envisioned achieving efficient $1/f$ noise suppression for EPR signals with ultrawide bandwidth by single sideband PSD as follows: Upon field modulation at the frequency ω_{mod} (e.g., 100 kHz), the upper sideband carrying all information of the target signal can be shifted out of the $1/f$ noise region. The aliasing lower sideband image is then removed from the upper sideband by an aliasing image-rejection procedure [Fig. 1(c)], affording a clean upper sideband. Afterward, the $1/f$ noise and the remaining lower sideband signal can be filtered out by an FFT high-pass filter, yielding an ultrawide single sideband (UWSSB) signal [Fig. 1(d)]. Single sideband demodulation is then applied to recover the $1/f$ noise-suppressed broadband EPR signal with high fidelity [Fig. 1(e)].

The key point in this detection method is eliminating the aliasing-image of the lower sideband, which was not achieved by the established B-PSD method. This is done by repeatedly generating the evolving radical signal $f(t)$ while manipulating the filed modulation phase (Fig. 2). The first kinetic event is triggered by laser pulse k while the field modulation is applied with an initial phase of φ_{mod}. The following event is triggered by a pulse $(k + 1)$ with a precisely controlled delay to ensure a $\pi/2$ shift on the field modulation phase. Two sets of modulated signals k and $(k + 1)$ are then generated, which consist of the same frequency components but with different initial phases. Compared with those in signal k [Fig. 2(a)], all components in signal $(k + 1)$ shift their phase by $\pi/2$ except the aliasing-image, which has a phase shift of $-\pi/2$. After applying a Hilbert transformation to signal $(k + 1)$, all its frequency components shift their phase by $-\pi/2$. As a result, the lower and upper sidebands become the same as those in signal k, while the aliasing-image part has a $-\pi$ phase shift to generate its inversed image [Fig. 2(b)]. The summation of signal k and Hilbert transformed signal $(k + 1)$ eliminates the overlapping lower sideband image to afford an aliasing image-free modulation signal [Fig. 2(c)]. This is followed by an FFT high-pass filter to remove the frequency components below ω_{mod}, leading to a clean UWSSB modulation signal.

B. Mathematics

The essential reconstruction of UWSSB signal from conventional field modulation-based EPR relies on repeatable kinetic events while precisely manipulating the initial phase of modulation as illustrated in Fig. 2. When a kinetic event is triggered by a laser pulse k and has an initial modulation phase of $\varphi_{mod,k}$, the modulated transient signal sampled from microwave bridge can be expressed as

$$S_k(t) = f(t) \times bF'(B_0)\cos(\omega_{mod}t + \varphi_{mod,k}) + N_{1/f,k}(t), \quad (2)$$

where $f(t)$ is the target transient signal, $F'(B_0)$ is the first-order derivative of the EPR absorption spectrum of the target radical at field strength B_0, b is the amplitude of field modulation, and $N_{1/f,k}(t)$ denotes $1/f$ noise. According to formula (1), we obtain the discreate form of the microwave bridge signal,

$$\begin{aligned} S_k(t) &= \sum a_i \cos(\omega_i t + \varphi_i) \times bF'(B_0)\cos(\omega_{mod}t + \varphi_{mod,k}) + N_{1/f,k}(t) \\ &= \sum \frac{1}{2}a_i bF'(B_0)\cos[(\omega_{mod} + \omega_i)t + (\varphi_{mod,k} + \varphi_i)] \\ &\quad + \sum \frac{1}{2}a_i bF'(B_0)\cos[(\omega_{mod} - \omega_i)t + (\varphi_{mod,k} - \varphi_i)]_{\omega_i \le \omega_{mod}} \\ &\quad + \sum \frac{1}{2}a_i bF'(B_0)\cos[(\omega_i - \omega_{mod})t + (\varphi_i - \varphi_{mod,k})]_{\omega_i > \omega_{mod}} + N_{1/f,k}(t), \end{aligned} \quad (3)$$

in which the first part represents the desired upper sideband signal, the second part corresponds to a part of the lower sideband with frequency components of the target signal (ω_i) below ω_{mod}, and the third one denotes the aliasing lower sideband image. The second kinetic event was triggered by the following pulse $(k + 1)$, such that the initial phase shifts to $\varphi_{mod,k} + \pi/2$, then the output signal become

$$\begin{aligned} S_{k+1}(t) &= \sum a_i \cos(\omega_i t + \varphi_i) \times bF'(B_0)\cos(\omega_{mod}t + \varphi_{mod,k} + \pi/2) + N_{1/f,k+1}(t) \\ &= \sum \frac{1}{2}a_i bF'(B_0)\cos[(\omega_{mod} + \omega_i)t + (\varphi_{mod,k} + \varphi_i + \pi/2)] \\ &\quad + \sum \frac{1}{2}a_i bF'(B_0)\cos[(\omega_{mod} - \omega_i)t + (\varphi_{mod,k} - \varphi_i + \pi/2)]_{\omega_i \le \omega_{mod}} \\ &\quad + \sum \frac{1}{2}a_i bF'(B_0)\cos\left[(\omega_i - \omega_{mod})t + \left(\varphi_i - \varphi_{mod,k} - \frac{\pi}{2}\right)\right]_{\omega_i > \omega_{mod}} + N_{1/f,k+1}(t). \end{aligned} \quad (4)$$

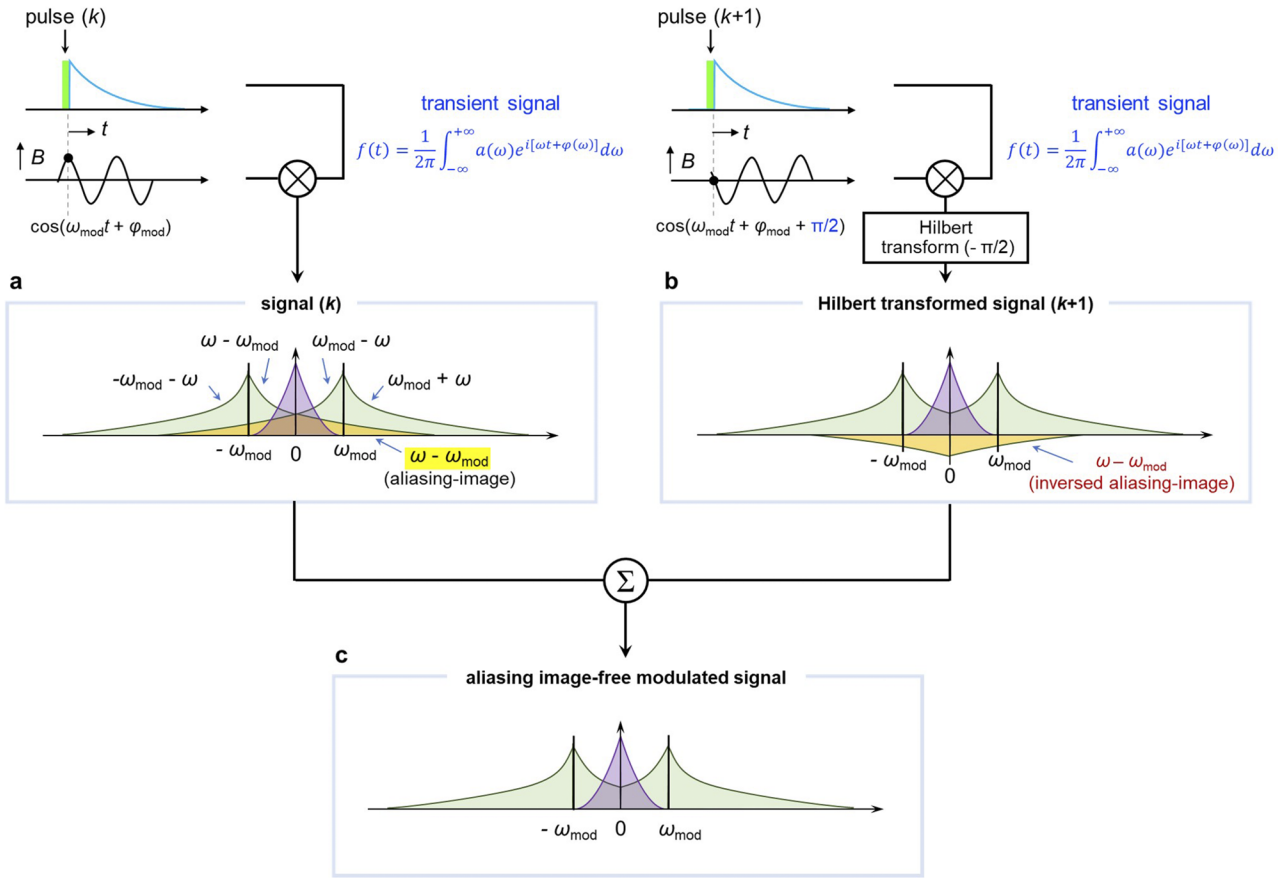

FIG. 2. Aliasing-image rejection via phase manipulations. (a) Modulated transient signal (k), (b) Hilbert transformed signal (k+1) with inversed aliasing-image signal, and (c) an aliasing image-free modulated signal.

A subsequent Hilbert transformation results in

$$\begin{aligned}\hat{S}_{k+1}(t) = &\sum \frac{1}{2} a_i b F'(B_0) \cos\left[(\omega_{\mathrm{mod}} + \omega_{\mathrm{i}})t + (\varphi_{\mathrm{mod},k} + \varphi_{\mathrm{i}})\right] \\ &+ \sum \frac{1}{2} a_i b F'(B_0) \cos\left[(\omega_{\mathrm{mod}} - \omega_{\mathrm{i}})t \right. \\ &\left. + (\varphi_{\mathrm{mod},k} - \varphi_{\mathrm{i}})\right]_{\omega_i \le \omega_{\mathrm{mod}}} \\ &+ \sum \frac{1}{2} a_i b F'(B_0) \cos\left[(\omega_{\mathrm{i}} - \omega_{\mathrm{mod}})t \right. \\ &\left. + (\varphi_{\mathrm{i}} - \varphi_{\mathrm{mod},k} - \pi)\right]_{\omega_i > \omega_{\mathrm{mod}}} + \hat{N}_{1/f,k+1}(t). \end{aligned} \tag{5}$$

The sum of $S_k(t)$ and $\hat{S}_{k+1}(t)$ is

$$\begin{aligned} S_k(t) + \hat{S}_{k+1}(t) = &\sum a_i b F'(B_0) \cos\left[(\omega_{\mathrm{mod}} + \omega_{\mathrm{i}})t \right. \\ &\left. + (\varphi_{\mathrm{mod},k} + \varphi_{\mathrm{i}})\right] + \sum a_i b F'(B_0) \\ &\times \cos\left[(\omega_{\mathrm{mod}} - \omega_{\mathrm{i}})t + (\varphi_{\mathrm{mod},k} - \varphi_{\mathrm{i}})\right]_{\omega_i \le \omega_{\mathrm{mod}}} \\ &+ N_{1/f,k+1}(t) + \hat{N}_{1/f,k+1}(t), \end{aligned} \tag{6}$$

in which the aliasing lower sideband image has been removed.

The desired upper sideband and lower frequency components, especially the $1/f$ noise, can be readily separable by using an FFT high-pass filter. As a consequence, the ultrawide single side band modulation signal now is fully reconstructed,

$$S_{UWSSB}(t) = \sum a_i b F'(B_0) \cos\left[(\omega_{\mathrm{mod}} + \omega_{\mathrm{i}})t + (\varphi_{\mathrm{mod},k} + \varphi_{\mathrm{i}})\right]. \tag{7}$$

Following single sideband demodulation is then performed to recover the target transient signal $f(t)$, which can be realized via either phase shifting method[20] or a modified lock-in detector that uses broadband averaging instead of a low-pass filter, as proposed by de Jager and van Wijk.[19]

It is worth noting that, if the modulation amplitude is increased with respect to the linewidth (i.e., over-modulation), higher order harmonics are created as well. Under this circumstance, the U-PSD is still able to cleanly recover the target signal because the higher harmonics will be easily canceled by an averaging procedure while varying the initial phase of field modulation. In principle, this unique feature can eliminate broadband interferences as well, such as strong impulsive RF noise from electronic devices or laser pulses (see the supplementary materialfor detailed discussions).

C. Simulation

In order to verify the validity of the EPR detection principle described above, LabVIEW-based computer simulations were carried out to examine the fidelity of the method for recovering signals with ultrawide bandwidth and to test its ability in $1/f$ noise suppression.

1. Recovery of signals with ultrawide bandwidth

An imagined unit step signal, which has infinite bandwidth, was selected as the target. To recover this type of signal using a PSD-based method, clean separation of the aliasing-image is essential.

A gated sine wave signal was chosen to simulate a unit step signal modulated with a 100 kHz sine wave function. Data in a 10 ms time period were acquired under 20 and 200 MSPS sampling rates, respectively. As shown in Fig. 3(a), in both cases, the U-PSD method is competent for recovering the step signal without noticeable distortions. Only when zooming in 1000 times, damping oscillations were observed. These distortions are caused by the Nyquist frequency-limited bandwidth, as the bandwidth of a step signal is infinite. This is consistent with decreasing trends both in amplitude and period of the damped oscillation while increasing the sampling rate [Fig. 3(b)]. These results clearly demonstrate the superior fidelity of our U-PSD protocol for recovering signals with ultrawide bandwidth.

2. 1/f noise suppression

Imagined EPR signals (a single Gaussian peak, 2σ = 1 mT) evolving rapidly (exponential rise or decay) within different time frames (10 μs, 10 ms, and 1000 ms) were chosen as the target signal to be detected. The ability of the present detection protocol to recover both the evolution kinetics of the signal and the peak shape was tested.

The output signal of the microwave bridge was generated by simulating a 100 kHz field modulation (amplitude = 0.5 mT) with appropriate sampling rates (200 MSPS for 10 μs period, 2 MSPS for 10 and 1000 ms periods), and increasing levels of $1/f$ noise (NL) were added to test the performance of $1/f$ noise suppression under different timescales. Two sets of data were acquired for each kinetic event with a $\pi/2$ modulation phase shift, and the target signal was recovered by the U-PSD algorithm described above. To obtain the evolution kinetics of the radical, the data were acquired under a fixed field strength (B_0), and decimations by averaging neighboring data points were performed to achieve a suitable time resolution for each kinetic curve. To acquire time-resolved EPR spectrum, a field scan was performed during data acquisition, and the intensity of the EPR signal at different field strengths was obtained by integration within the corresponding time range.

The simulation results showed that our U-PSD method is competent for the detection of transient EPR signals in different timescales. Under a fast kinetic regime [Fig. 4(a)], the present method matches the performance of the direct detection method, which recovers the kinetic trace with a high time resolution as well as well-resolved transient first-order differential EPR spectra. To our delight, under intermediate and slow kinetic regimes [up to 1000 ms, Figs. 4(b) and 4(c)] where the $1/f$ noise dominates and the DD-TREPR fails,[6] the present method is also able to recover EPR signals with high fidelity and sensitivity. This indicated that the present method exhibits outstanding $1/f$ noise suppression performance as anticipated.

III. U-PSD TREPR INSTRUMENTATION

To further demonstrate the feasibility of our U-PSD method, the realization of the TREPR instrumentation based on this technique has been conducted in our laboratory. The instrumental design was based on a commercial SS CW-EPR spectrometer (Magnettech MS5000) with the integration of sample delivery & excitation systems, and a U-PSD module, which includes additional units for data acquisition, timing sequence control, and U-PSD algorithm.

Figure 5 shows the block diagram of the experimental setup for our U-PSD TREPR system. The magnet and microwave systems of the commercial spectrometer were used without modification (shown in the blue dashed rectangle). Essential hardware modifications have been made and can be described as follows:

(1) The coupling iris of the TE_{102} rectangular cavity resonator was modified to ensure successful critical coupling at low Q conditions (i.e., Q = 500–1000).
(2) Sample delivery system was designed to facilitate through-axis photoexcitation. A sample tube (i.d. = 2.0 mm) and a coaxial quartz fiber optic (o.d. = 1.9 mm) were used, which leaves a 10 mm light pathlength through the cavity. The sample tube is isolated from the atmosphere by a tube Dewar, and temperature control was realized using a liquid nitrogen temperature controller. A PTFE micro piston pump or a syringe pump was used to make the sample solution flow through the sample tube, which avoids rapid sample depletion and unwanted product accumulation.

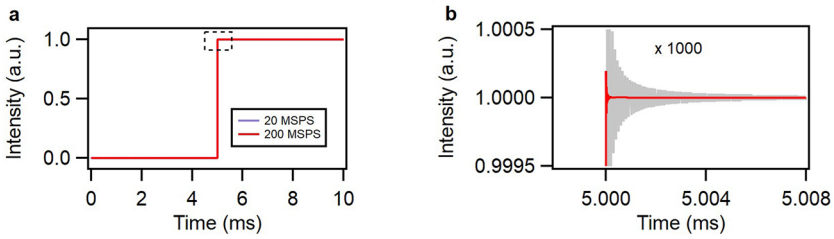

FIG. 3. The fidelity of the U-PSD examined with a unit step function under various sampling rates. (a) The recovered step signals by the U-PSD method at a sampling rate of 20 and 200 MSPS and (b) damping oscillations observed when zooming in 1000 times at the corner of the step signal.

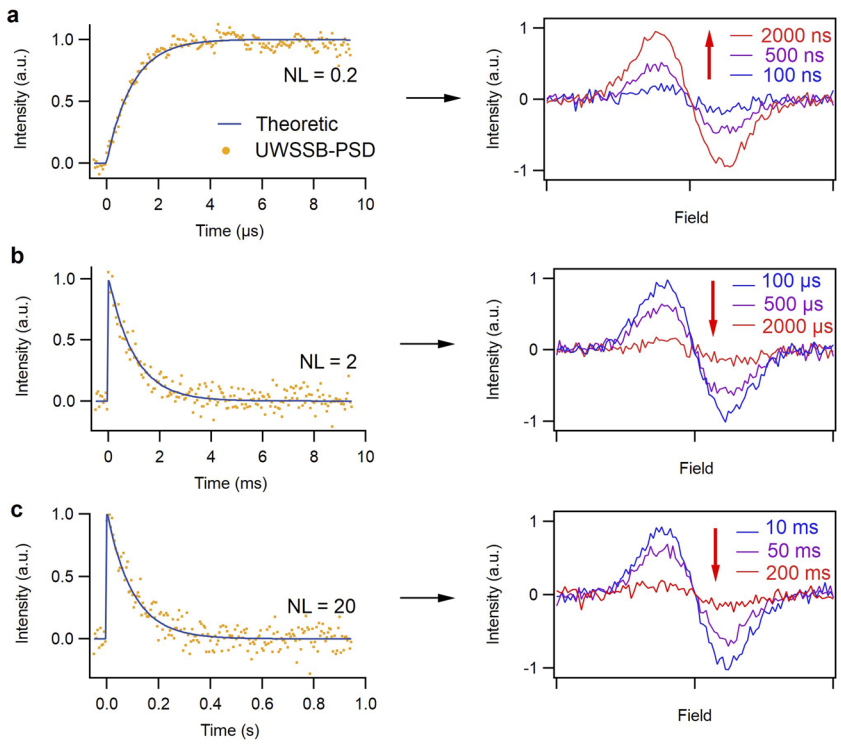

FIG. 4. The 1/*f* noise suppression ability of the U-PSD algorithm within different timescales verified by simulations. Exponential rise or decay signals and kinetic spectra in the timescales of (a) 10 μs, (b) 10 ms, and (c) 1 s.

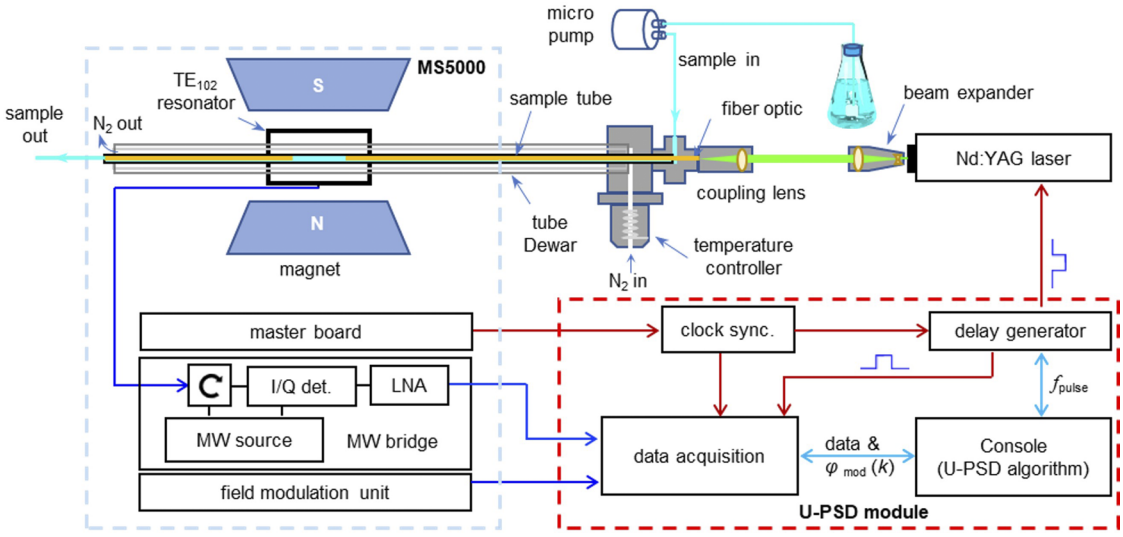

FIG. 5. Block diagram for the U-PSD TREPR system.

(3) Sample excitation was done by a DPSS Nd:YAG laser with a repetition rate of 0–100 Hz, and the third harmonic at 355 nm wavelength was used. Given the long excitation pathlength (10 mm) along the sample tube, the pulse energy required in our system is less than 5 mJ/pulse, which is an order of magnitude lower than the commonly used flat cell and perpendicular beam excitation system.[6] Coupling of the laser beam into fiber optic is crucial for efficient sample excitation. To guarantee the excitation efficiency, a parallel beam coming out of the fiber optic is desired. Therefore, one end of the quartz fiber optic was fabricated into a convex surface with a radius of curvature of 10 mm. Together with the beam expander and coupling lens, a satisfactory near-parallel excitation beam was obtained.

(4) The data acquisition system was modified to allow for direct readout of signals from the microwave bridge, field modulation unit, hall sensor, and instrumental system clock. Data acquisition was accomplished with a PCIe-based 2 channel 250 MSPS 16-bit high speed ADC card. To fully use the dynamic range of the ADC module, a band-pass filter of 50 kHz–10 MHz and a preamplifier with a 350 MHz bandwidth were used.

(5) A Stanford DG645 digital delay generator provided the trigger signals both for the laser and the data acquisition system. A signal generator was used to convert a 600 kHz clock signal (on board sampling clock from MS5000) to a 10 MHz time base for the delay generator and the data acquisition module. As system clocks have been synchronized between the EPR instrument, data acquisition system, and delay generator, the phase shift between adjacent kinetic events was realized by the laser pulse delay setting to 10 $(n + 1/4)$ μs, where the integer value n is adjusted to adapt the repetition rate of the laser pulse. In case higher harmonics or other electromagnetic interferences are present, averaging among different groups of kinetic events while varying the initial phase of field modulation is required (see the supplementary material for detailed discussion).

The key algorithm and system control were realized with the LabVIEW software. Because the bandwidth of the system is determined by the cavity (~5–10 MHz at Q = 500–1000), software down sampling (averaging) of the initial 250 MSPS data flow to 25 MSPS was conducted before further processing to gain higher vertical resolution. Phase correction is also required to calibrate the phase shift produced by the band-pass filter, and the calibration curve was obtained with a Tektronix DSO64 oscilloscope and a signal generator.

IV. RESULTS AND DISCUSSION

A. Performance of U-PSD TREPR in a model radical reaction

The laser flash photolysis (LFP) of benzophenone (BP) in isopropyl alcohol (IPA) was selected as a testing ground to assess the performance of the developed U-PSD TREPR instrument. It has been established that, upon laser pulse excitation, the excited state of BP abstracts a hydrogen atom immediately from the C–H bond of IPA, which generates two radicals: a reactive and fast decaying IPA radical, and a relatively stable and slowly decaying benzhydrol radical (Fig. 6).[21] Previous DD TREPR studies on this system merely observed the intense CIDEP signals of two radicals, while the much less intense spin-equilibrium state signals of the IPA radical and the benzhydrol radical were not observable.[22,23] Our aim was to observe both the CIDEP and the thermal-equilibrium state signals of the two radicals, as well as trace their evolution with a high time resolution.

Using our U-PSD TREPR instrument, a typical first-order differential CIDEP spectrum was obtained by performing a field scan and applying an integration width of 1 μs directly after the laser pulse [Fig. 6(b), gate: 0–1 μs]. Signals corresponding to both the IPA radical (●) and the benzhydrol radical (▲) were observed. The IPA radical showed emission peaks in the low field region and absorption peaks in the high field region, while the central peak was not clearly visible, which agreed with the reported transient spectrum.[22] To our delight, the spectrum was clearly resolved to show the hyperfine couplings in both radicals. The evolution of the signal of the IPA radical [the peak marked with * in Fig. 6(b)] can be traced at a fixed field strength, and its CIDEP dynamics were followed with sufficiently high time resolution [~40 ns, Fig. 6(c)]. Acquisition under different MW powers verified the CIDEP nature of this signal, as the frequency of the Rabi (or Torrey) oscillation is proportional to the square root of the applied MW power.

The high sensitivity of the acquired data allowed us to take a closer look into the tailing part of the signal where the CIDEP dynamics ended [Fig. 6(d)]. It appeared that, after the rapidly evolving CIDEP dynamics (0–5 μs), we were able to observe that the IPA radical underwent a slower decay process, which was not clearly observed in previous TREPR studies of the same system. We assigned this to the chemical decay of IPA radical with a Boltzmann distribution of spin state. A full transient EPR spectrum acquired at the post-CIDEP period (gate: 5–40 μs) confirmed this assignment, which showed characteristic peaks of the IPA radical under thermal equilibrium [Fig. 6(e), including the central peak invisible in the CIDEP spectrum, marked with #].[24] Notably, the EPR signals at this stage were far less intense than the CIDEP signals, and the observation time window exceeded the applicable one of the DD TREPR, but the present U-PSD TREPR instrument still worked well. Moreover, the kinetics of the chemical decay of IPA radical can be nicely followed within a wider time window [3–120 μs, Fig. 6(f)]. The fast kinetic spectra of the CIDEP signals [Fig. 6(g), left panel] clearly demonstrate the superior time resolution of this spectrometer, and the time response is well consistent with the risetime (~40 ns) determined by the microwave photoconductivity (TRMC) experiment (see the supplementary material for details). Furthermore, in the post-CIDEP stage, transient spectra reflecting the chemical decay process can be easily acquired as well [Fig. 6(g), right panel], which is rather useful for mechanistic study in radical chemistry.

We further examined the signals of more stable benzhydrol radicals at the center region of the acquired transient EPR spectrum (Fig. 7). It was found that at early delay times (0–1 μs), the CIDEP signal of this radical dominated [Fig. 7(a)], and later, it returned to thermal equilibrium and exhibited a normal EPR spectrum [Fig. 7(b)], which is well consistent with the simulated spectrum [Fig. 7(c)] based on the literature reported hyperfine

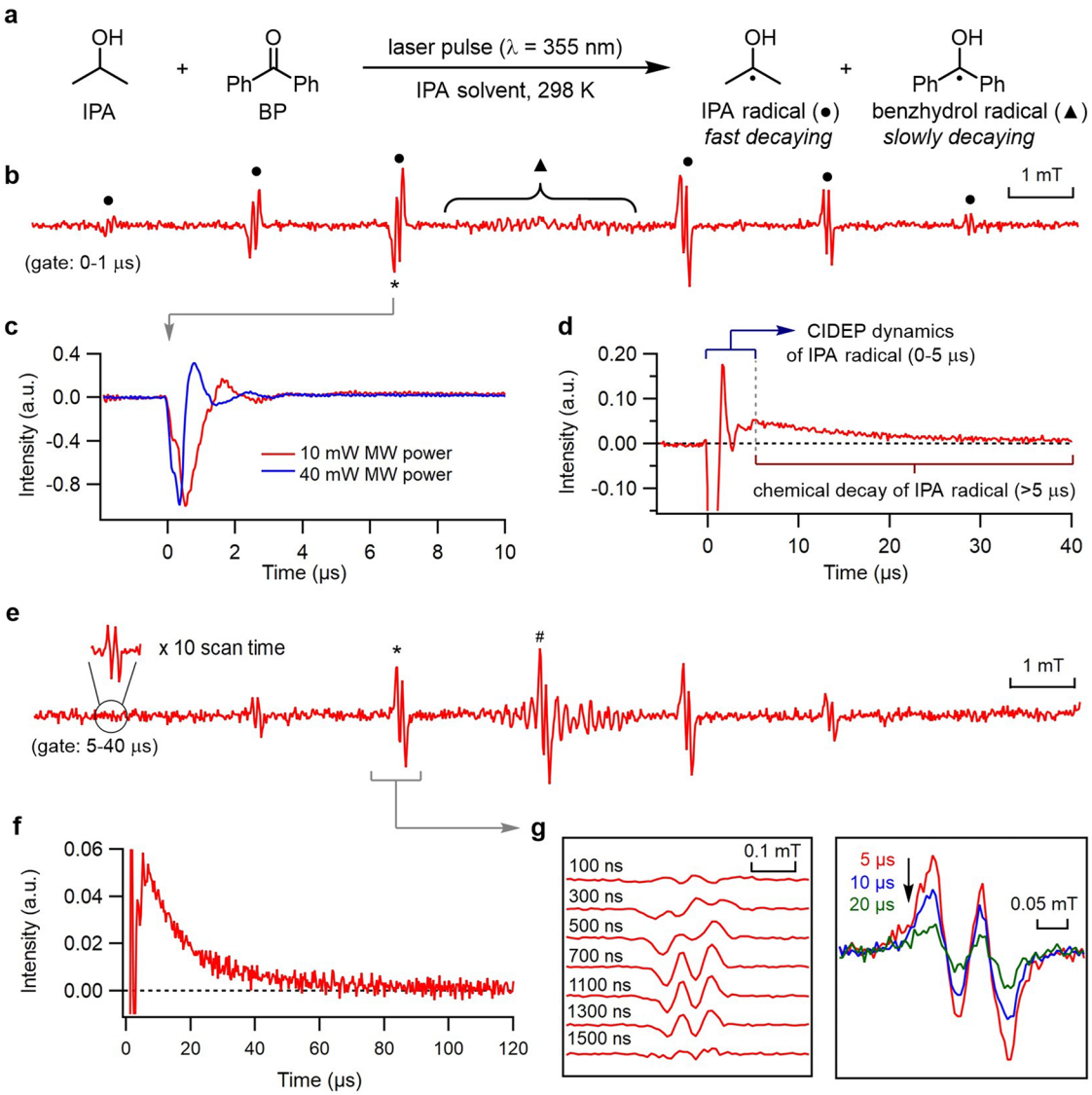

FIG. 6. Study on the Photolysis of BP in IPA by U-PSD TREPR. (a) Testing system of benzophenone (BP) in isopropyl alcohol (IPA), (b) the CIDEP spectra of the IPA radical (•) and the benzhydrol radical (▲) acquired with a gate of 0–1 μs, (c) CIDEP dynamics by monitoring the designated peak (*) at 10 and 40 mW microwave power, respectively, (d) zoomed kinetic trace in (c) at 10 mW microwave power showing both the CIDEP kinetics and chemical decay of the IPA radical, (e) the characteristic spectra of the IPA radical and BP radical under thermal equilibrium spin state acquired with a gate of 5–40 μs, (f) zoomed kinetic trace in (c) at 10 mW microwave power showing the chemical decay of IPA radical in the timescale of 120 μs, and (g) the evolution of the CIDEP spectra (left panel) and the corresponding thermal equilibrium spectra in the post-CIDEP stage (right panel) of a specific set of peaks.

coupling parameters obtained from steady-state measurements.[25] The CIDEP dynamics of this radical can also be traced by monitoring the designated peak [marked with * in Fig. 7(a)], in which the Rabi oscillation was clearly visible [Fig. 7(d)]. The instrument was able to trace the long-term evolution of this radical, and kinetic profiles at different peak positions [marked with @ and # in Fig. 7(a)] provided consistent kinetic information, which indicated that the chemical decay of this radical required a few milliseconds and was much slower than the IPA radical [Fig. 7(e)].

Overall, by employing the LFP of BP in IPA as a model, the capacity of the U-PSD TREPR instrument in the detection of transient radicals has been demonstrated. The model system contains radical species with distinct evolution kinetics covering a rather wide timescale (fast CIDEP dynamics within microseconds, intermediate decay within hundreds of microseconds, and slow decay within milliseconds). The present instrument was proven competent for obtaining both the transient EPR spectra and kinetic traces of those radicals within a wide time window. Importantly, only one

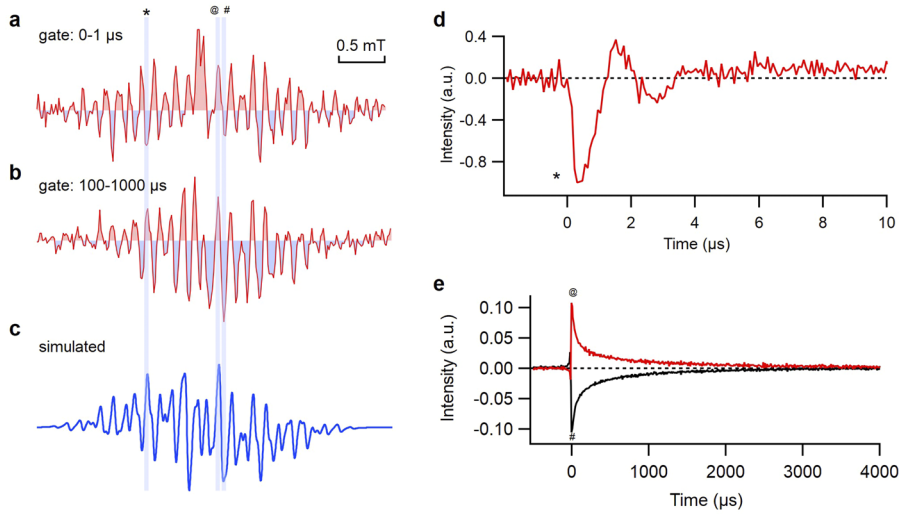

FIG. 7. Transient EPR spectra and kinetic traces of benzhydrol radical. (a) The CIDEP spectrum of BP radical in the first microsecond, (b) the thermal equilibrium spectrum of BP radical with a gate of 100–1000 μs, (c) the simulated spectrum, (d) the CIDEP dynamics of the BP radical, and (e) long-term evolution of the BP radical monitored at the designated peaks @ and #.

kinetic acquisition run is required to generate kinetic traces with various time windows and time resolutions [i.e., Figs. 6(c), 6(d), 6(f), 7(d), and 7(e)], showcasing the advantage of the U-PSD method in detecting EPR signals with an ultrawide bandwidth.

B. Discussions

The U-PSD TREPR technique developed in our current research demonstrated significantly improved sensitivity compared to traditional DD TREPR. We observed that none of the previously reported DD TREPR studies on the same model reaction system produced well resolved EPR spectra in the much less intense thermal equilibrium spin state. Our own comparison of the direct detection approach, using identical hardware configurations, further confirmed that it only yielded CIDEP spectra, with the EPR signal in the post-CIDEP stage being invisible due to high levels of noise. A quantitative evaluation revealed that the U-PSD method increased the signal-to-noise ratio (SNR) over the DD method by factors of 1.5, 25, and 100 within the timescales of 1, 40, and 1000 μs, respectively. (see the supplementary material for detailed information).

Another advantage of the U-PSD TREPR is its high spectral resolution. Traditional TREPR methods typically provide time-resolved integrated spectra due to their direct detection nature. In contrast, our method can generate first-order derivative differential EPR spectra with a high time resolution, which is extremely useful for characterizing the structure of transient radical species [e.g., Figs. 6(b), 6(e), 7(a), and 7(b)]. This task is quite challenging for traditional DD TREPR methods. To the best of our knowledge, the transient spectrum with hyperfine structural characteristics of the photogenerated BP radical under a thermal equilibrium spin state has not been reported in previous TREPR studies.[26,27]

It is worth mentioning that having the microwave frequency locked precisely to the resonance frequency of the resonator is crucial for long-time acquisitions. This is a rather challenging technical requirement for DD TREPR because the highly effective alternating current automatic frequency control (AC-AFC) used in SS CW-EPR is not applicable in transient detections, and a less stable DC-AFC has to be used. On the contrary, the present U-PSD TREPR is fully compatible with AC-AFC, which is clearly demonstrated by the above long-time kinetic acquisitions [in a duration of ~100 min, fig. 7(e), especially in the case where peaks with narrow linewidths should be followed. While we must admit that the AC-AFC technique is not perfect. Although AC-AFC is the most commonly used technique in EPR, to some extent, it tends to distort the absorption signal with the dispersion component due to the inherent limitation of the frequency lock mechanism, especially when saturation of the microwave absorption occurs. This issue might be solved by increasing the time constant of the lock-in detection for the AC-AFC feedback, which can be considered when designing a new U-PSD based TREPR system in the future.

V. CONCLUSION

In conclusion, this study validated the feasibility of the U-PSD technique and demonstrated the superior performance of the TREPR instrument prototype based on this technique in studying complex chemical systems containing various transient radicals:

(1) The U-PSD method enables the successful extraction of weak signals with ultrawide bandwidth from extremely noisy environments containing massive $1/f$ noise. The demonstration system performed well within a detection time window of ~5 ms (which could be further extended) under a high time resolution (~40 ns, cavity-limited). These combined features allow for the tracing of weak signals of fast-evolving radicals under thermal equilibrium, which is rather difficult with previous TREPR techniques.

(2) The U-PSD method affords better spectral resolution compared with DD TREPR, owing to the differential nature of the PSD-based technique. This represents a unique advantage in providing more detailed structural information on short-lived radical species, which is particularly beneficial for the study of complex radical reactions.
(3) The TREPR spectrometer based on the U-PSD technique requires minimum hardware modifications on a conventional CW-EPR, leaving the microwave system and the field scan/modulation system untouched. Therefore, it enables an advanced TREPR technique at a reasonable cost.

SUPPLEMENTARY MATERIAL

Details of the U-PSD TREPR setup, data acquisition, and post-processing, as well as performance tests.

ACKNOWLEDGMENTS

Dedicated to Professor Dennis Curran on the occasion of his 70th birthday. We thank Dr. Zhifu Shi and the Professors Ming-Tian Zhang, Oliver S. Wenger, and Herbert Mayr for helpful discussions. This work was supported by Tsinghua University Dushi Program. We acknowledge the National Natural Science Foundation of China (Grant No. NSFC 22193011) and the Haihe Laboratory for Sustainable Chemical Transformations for financial support.

AUTHOR DECLARATIONS

Conflict of Interest

The authors have no conflicts to disclose.

Author Contributions

Shixue Zhang: Data curation (equal); Formal analysis (supporting); Investigation (equal); Methodology (supporting); Software (equal); Writing – review & editing (equal). **Shengqi Zhou**: Data curation (supporting); Investigation (supporting); Software (supporting); Writing – review & editing (supporting). **Jianqing Qi**: Data curation (supporting); Investigation (supporting); Software (supporting); Writing – review & editing (supporting). **Lei Jiao**: Formal analysis (equal); Investigation (supporting); Methodology (supporting); Software (equal); Validation (equal); Writing – original draft (equal); Writing – review & editing (equal). **Xingwei Guo**: Conceptualization (lead); Data curation (equal); Formal analysis (equal); Funding acquisition (lead); Investigation (equal); Methodology (lead); Project administration (lead); Software (equal); Supervision (lead); Validation (equal); Writing – original draft (equal); Writing – review & editing (equal).

DATA AVAILABILITY

The data that support the findings of this study are available from the corresponding author upon reasonable request.

REFERENCES

[1] S. S. Kim and S. I. Weissman, J. Magn. Reson. **24**, 167 (1976).
[2] S. Weber, eMagRes **6**, 255 (2017).
[3] C. E. Tait, P. Neuhaus, H. L. Anderson, and C. R. Timmel, J. Am. Chem. Soc. **137**, 6670 (2015).
[4] E. Stavitski, A. Berg, T. Ganguly, A. Mahammed, Z. Gross, and H. Levanon, J. Am. Chem. Soc. **126**, 6886 (2004).
[5] X. Zhang, Y. Hou, X. Xiao, X. Chen, M. Hu, X. Geng, Z. Wang, and J. Zhao, Coord. Chem. Rev. **417**, 213371 (2020).
[6] M. D. E. Forbes, L. E. Jarocha, S. Y. Sim, and V. F. Tarasov, Adv. Phys. Org. Chem. **47**, 1 (2013).
[7] C. Chatgilialoglu and A. Studer, *Encyclopedia of Radicals in Chemistry, Biology and Materials* (John Wiley and Sons, 2012).
[8] A. J. Gillett, A. Privitera, R. Dilmurat, A. Karki, D. Qian, A. Pershin, G. Londi, W. K. Myers, J. Lee, J. Yuan, S.-J. Ko, M. K. Riede, F. Gao, G. C. Bazan, A. Rao, N. Nguyen, D. Beljonne, and R. H. Friend, Nature **597**, 666 (2021).
[9] E. Karatekin, B. O'Shaughnessy, and N. J. Turro, Macromolecules **31**, 7992 (1998).
[10] M. Flores, A. Savitsky, E. C. Abresch, W. Lubitz, and K. Möbius, in *Photosynthesis. Energy from the Sun. 14th International Congress on Photosynthesis* (Springer, 2008), p. 59.
[11] O. Krumkacheva, M. Tanabe, S. Yamauchi, M. Fedin, S. R. A. Marque, and E. Bagryanskaya, Appl. Magn. Reson. **42**, 29 (2012).
[12] M. Jager and J. R. Norris, J. Phys. Chem. A **106**, 3659 (2002).
[13] A. M. Brughand and M. D. E. Forbes, Chem. Sci. **11**, 6268 (2020).
[14] K. A. McLauchlan and D. G. Stevens, J. Chem. Phys. **87**, 4399 (1987).
[15] D. Goldfarb and S. Stoll, *EPR Spectroscopy: Fundamentals and Methods* (John Wiley & Sons, 2018).
[16] B. Smaller, J. R. Remko, and E. C. Avery, J. Chem. Phys. **48**, 5174 (1968).
[17] G. E. Smith, R. E. Blankenship, and M. P. Klein, Rev. Sci. Instrum. **48**, 282 (1977).
[18] P. W. Atkins, K. A. McLauchlan, and A. F. Simpson, J. Phys. E: Sci. Instrum. **3**, 547 (1970).
[19] P. A. de Jager and F. G. H. van Wijk, Rev. Sci. Instrum. **58**, 735 (1987).
[20] D. E. Norgaard, P. IRE **44**, 1735 (1956).
[21] A. Demeter, B. László, and T. Bérces, Ber. Bunsenges. Phys. Chem. **92**, 1478 (1988).
[22] A. D. Trifunac and J. R. Norris, Chem. Phys. Lett. **59**, 140 (1978).
[23] A. D. Trifunac, M. C. Thurnauer, and J. R. Norris, Chem. Phys. Lett. **57**, 471 (1978).
[24] R. Livingston and H. Zeldes, J. Chem. Phys. **44**, 1245 (1966).
[25] R. Wilson, J. Chem. Soc. B **1968**, 84.
[26] J. R. Woodward, T.-S. Lin, Y. Sakaguchi, and H. Hayashi, Mol. Phys. **100**, 1235 (2002).
[27] A. Jones and J. R. Woodward, Mol. Phys. **104**, 1551 (2006).